PHYSICAL REVIEW B VOLUME 35, NUMBER 3 15 JANUARY 1987-II

Conduction band of Si-Ge_xSi_{1-x} superlattices using the envelope-function approximation

C. M. de Sterke and D. G. Hall
The Institute of Optics, The University of Rochester, Rochester, New York 14627
(Received 6 May 1986; revised manuscript received 10 November 1986)

We have calculated the structure of the conduction band in Si-Ge_xSi_{1-x} superlattices using the envelope-function approximation, neglecting the transverse directions. Our description of the bulk materials is valid throughout the Brillouin zone along one direction and consequently takes the multiple minima of the conduction band into account. We find that in contrast to those for superlattices made from direct-band-gap semiconductors, the energy bands for Si-Ge_xSi_{1-x} superlattices exhibit a splitting that we assign to the interaction between the two conduction-band minima along the superlattice direction. It is shown that in the limit of infinitely deep wells, the splitting depends sinusoidally on the well width.

I. INTRODUCTION

The original paper on semiconductor superlattices (SL's) by Esaki and Tsu (1970),[1] generated widespread interest in the electrical and optical properties of these novel solid-state structures. SL's formed from alternating layers of GaAs and $Al_xGa_{1-x}As$ have attracted the greatest attention, but it is well known that SL's can be fabricated from other III-V materials, II-VI materials, and silicon and germanium as well (for recent reviews, see Refs. 2 and 3). The large lattice mismatch ($\sim 4\%$) between silicon and germanium hampers the formation of dislocation-free interfaces, but recent work has shown that good-quality Si-Ge_xSi_{1-x} heterostructures can be obtained by choosing appropriate growth conditions.[4-7]

We are aware of only two previously published approaches to band structure calculations for silicon-based SL's. The first of these was published in 1975,[8] and is in fact an extension of the Kronig-Penney model. Experience with GaAs-$Al_xGa_{1-x}As$ structures has taught that the validity of these kinds of models is very limited. More recently, a series of papers has appeared in which the band structure is calculated using an empirical tight-binding method.[9-11] This is considered to be the most reliable method for GaAs-$Al_xGa_{1-x}As$ structures,[12] but requires rather large computations.

The envelope-function approximation (EFA) is yet another method that has been developed for GaAs-based SL's.[13-16] In this method, the band structure of the bulk materials is described using the $\mathbf{k}\cdot\mathbf{p}$ method[17] and the bands of the SL are then obtained by applying the effective mass approximation (EMA).[18] Since both GaAs and $Al_xGa_{1-x}As$ have a direct band gap in the middle of the Brillouin zone (BZ) (unless x is too large), a correct description of the band structure of just the region around the Γ point suffices to obtain the bands of the associated SL. In this case, therefore, the Kane formalism[19] is used, and a rather simple dispersion relation can be derived, which is similar in shape to the results of a straightforward Kronig-Penney calculation. By comparing the results using the EFA to results based on the tight-binding calculation, it has been shown that the EFA has a wide range of validity.[12]

In this paper we describe the application of the EFA to Si-Ge_xSi_{1-x} heterostructures. We will neglect crystal momentum in directions transverse to the SL axis. Our work is an extension of the III-V work in the sense that a description of the bands valid in the entire BZ is used. This is necessary to take the equivalent conduction-band minima in bulk silicon properly into account. In fact, we only consider the minibands formed out of this lowest conduction band in the present paper, as this full BZ description is the essential new feature of our method. The full BZ description makes the calculations more complicated; we have not been able to find a simple dispersion relation, but we are able to find analytic solutions which require very modest computation.

The contents of this paper are as follows: In Sec. II we discuss our method and we derive the basic equations. In Sec. III we apply the formalism to Si-Ge_xSi_{1-x} SL's; we observe that, in contrast to the case of GaAs-$Al_xGa_{1-x}As$, the energy levels are split. In Sec. IV we discuss the results and, in order to explain the splitting of the levels qualitatively, we derive a simple equation to calculate the energy levels in an infinitely high potential well made of indirect band gap material. Conclusions are summarized in Sec. V. In this paper we will use the term "superlattice" (SL) but our analysis applies to multiple quantum wells as well.

II. DESCRIPTION OF THE METHOD

The EFA starts out with a description of the bands of the two constituent materials in the relevant part of the BZ using the $\mathbf{k}\cdot\mathbf{p}$ method.[17] In this method, the energy of the bands at a certain value of the crystal momentum $\mathbf{k}$ is given by the solution of an algebraic eigenvalue equation. For example, Cardona and Pollak[20] have shown that, for silicon and germanium, the Δ_1 bands ([100] direction), to which the lowest conduction band in silicon belongs, are given as the eigenvalues of the matrix

 ©1987 The American Physical Society

$$\begin{vmatrix} E(\Gamma_{15})+k_x^2 & Tk_x & T'k_x \\ Tk_x & E(\Gamma_1^u)+k_x^2 & 0 \\ T'k_x & 0 & E(\Gamma_1^l)+k_x^2 \end{vmatrix} \quad (1)$$

(atomic units are used throughout the paper). The values of the energy bands at the Γ point, in increasing order are $E(\Gamma_1^l)$, $E(\Gamma_{15})$, $E(\Gamma_1^u)$, and the momentum matrix elements T and T' are given in the above-mentioned paper.[20] In this so-called three-band model, the middle band with energy $E(\Gamma_{15})$ at $k=0$ is the lowest conduction band. The band mixing for $k \neq 0$ is described by the eigenvectors of Eq. (1).

In order to introduce the SL environment, we use the EMA (Ref. 18). In this method, **k** is replaced by $-i\nabla$, which turns algebraic equations into differential equations. The eigenfunctions of these equations now represent an envelope of the wave function. Since linear-algebraic equations turn into linear-differential equations, the solution in the bulk material is a superposition of plane waves and evanescent waves. The wave numbers can be found by replacing $-i\nabla$ again by **k** and solving for **k**, given a value for the energy. Both real and imaginary as well as complex values for **k** will be found in general, giving rise to the so-called complex band structure.[21-23] Notice that this procedure is the opposite of that described earlier, where the energy followed after picking **k**.

We now apply the above described procedure to Eq. (1). This yields a set of three coupled second-order linear-differential equations. Choosing a value for the energy, the so obtained characteristic equation will be a cubic equation in k^2, so that six roots will be found, arranged in pairs of **k** and $-$**k**. For silicon, the solutions are given in Fig. 1. Note that since just the bands following from Eq. (1) are shown, this is only a part of the entire complex band structure. For a more complete version, see Fig. 5 of Chang and Schulman.[23] The short-dashed solutions in this figure are spurious. They show up for reasons described by Chang and Schulman[23] and by Schuurmans and 't Hooft.[16] What concerns us now is that these solutions have no physical significance but nevertheless will be treated in the same manner as the true physical solutions. This reduces the confidence in the physical significance of solution as a whole.

We will rid ourselves of the spurious solutions in a similar way as Schuurmans and 't Hooft[16] did. We will neglect the free-electron mass in the lowest of the three bands described by Eq. (1). This means that the k^2 term in the 3,3 element in Eq. (1) has to be dropped and that the parameters have to be adjusted. The characteristic equation of the matrix now turns into a quadratic equation in k^2, thus yielding four solutions instead of six. Obviously the description of the lower band will now be quite poor, but that does not concern us as long as the interaction with the band we are interested in, the middle band, is well represented. Applying the EMA, and turning **k** into $-i\nabla$, the following set of differential equations results:

$$\left[E(\Gamma_{15})-\frac{d^2}{dx^2}\right]F_1 - iT\frac{d}{dx}F_2 - iT'\frac{d}{dx}F_3 = EF_1 , \quad (2a)$$

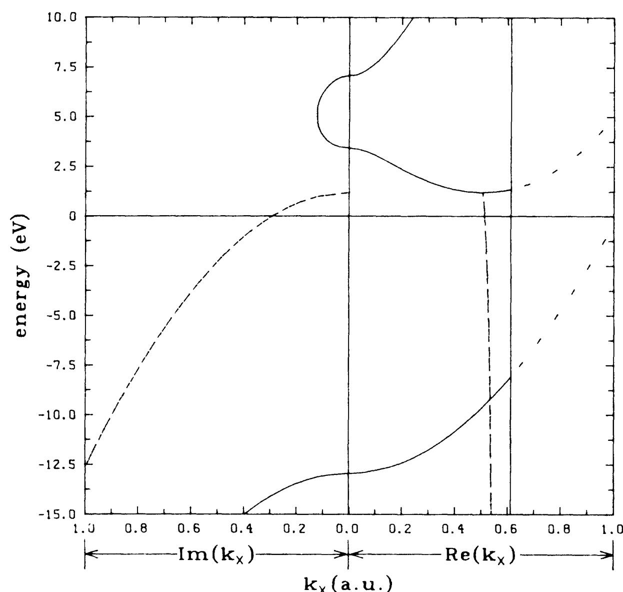

FIG. 1. Part of the complex band structure for Si in the [100] direction as following from the **k**·**p** method. Only Δ_1 bands are shown. The right-hand side of the figure gives the real part of **k**, the left-hand side gives the imaginary part. The vertical line at $k_x \approx 0.6$, indicates the edge of the Si Brillouin zone. Solid lines denote purely real bands (right-hand side) and purely imaginary bands (left-hand side). The long-dashed lines indicate complex conjugate bands and the short-dashed lines indicate the spurious bands.

$$-iT\frac{d}{dx}F_1 + \left[E(\Gamma_1^u)-\frac{d^2}{dx^2}\right]F_2 = EF_2 , \quad (2b)$$

$$-iT'\frac{d}{dx}F_1 + E(\Gamma_1^l)F_3 = EF_3 . \quad (2c)$$

By substituting F_3 from the bottom equation into the top line, we are left with two coupled equations. Hence, we effectively make use now of a two-band model.

The conventional way of solving this system for a SL is to match the solutions in each of the two materials and their first derivatives at the two boundaries, and to apply the Bloch condition. In our case, this would yield an 8×8 secular equation that has to be solved for every value of the energy. A more convenient way of solving Eq. (2) with the appropriate boundary conditions is the transfer matrix technique, which has been widely used in connection with one-band models.[24,25] Using the transfer matrices and given the envelope functions and their first derivative at an arbitrary position in the superlattice, it is possible to find them anywhere. The method requires transfer matrices for each of the materials and for the interfaces. The calculation to obtain the transfer matrix for a given material is conceptually very straightforward but algebraically extremely tedious. An outline of the method and the transfer matrix itself are given in the Appendix.

We also need to know the behavior of the envelope functions and their first derivatives upon passing an interface. In the EMA, the wave function in the perturbed

crystal is expanded in terms of wave functions in the unperturbed crystal. In the present work we write the SL wave function as a linear combination of the periodic part of the bulk wave functions at Γ. To be consistent therefore, these have to be the same in the two constituent materials. Although this is not strictly true, the similarity between Si and Ge assures that this assumption is not badly violated. That the periodic part of the wave functions at Γ must be equal, in turn requires that T and T' have to be the same. It has been shown that it also implies that the envelope functions are continuous at the interfaces.[26]

The connection rule for the derivatives of the envelope functions can be found by eliminating F_3 from Eqs. (2a) and (2c). This gives

$$\left[E(\Gamma_{15})-\frac{d^2}{dx^2}\right]F_1-iT'\frac{d}{dx}F_2+(T')^2\frac{d}{dx}\frac{1}{E(\Gamma_1^l)-E}\frac{d}{dx}F_1=0\ . \quad (3)$$

Integration of this expression over an interface, keeping in mind that F_1 and F_2 are continuous, now gives the connection rule:

$$\left[1-\frac{(T')^2}{E(\Gamma_1^l)-E}\right]\frac{d}{dx}F_1$$

is continuous over an interface. Integrating the remaining Eq. (2b) in a similar way shows simply that $(d/dx)F_2$ has to be continuous over an interface. These connection rules can be written in the form of a diagonal matrix that operates on the vector with components given in Eq. (A5):

$$\begin{bmatrix} 1 & 0 & 0 & 0 \\ 0 & 1 & 0 & 0 \\ 0 & 0 & \dfrac{1-(T')^2/[E(\Gamma_1^l)^A-E]}{1-(T')^2/[E(\Gamma_1^l)^B-E]} & 0 \\ 0 & 0 & 0 & 1 \end{bmatrix} \quad (4)$$

(for transfer from material A to material B). This transfer matrix for an interface, together with the matrix for transfer through the materials given in Eq. (A6), allow us to determine the envelope functions anywhere in the structure. To propagate the envelope functions over one period of the SL, the two types of transfer matrices have to be multiplied in the appropriate order.

We can now finally obtain the band structure by imposing the Bloch condition which requires that

$$\mathbf{F}(x+d)=e^{iqd}\mathbf{F}(x)\ , \quad (5)$$

where $\mathbf{F}$ is given in Eq. (A5), d is the period of the SL, and q is a real number that signifies the crystal momentum in the SL. This means that we have to determine the eigenvalues of the product matrix over a single period; eigenvalues with unit magnitude correspond to allowed solutions. An elegant way to find the eigenvalues can be devised by realizing that since the positive and negative x directions are fully equivalent; given that $\exp(iQ_1)$ is an eigenvalue (Q_1 is an arbitrary complex number), $\exp(-iQ_1)$ must be an eigenvalue as well. Hence, the four eigenvalues of the product matrix can be written as $\exp(iQ_1)$, $\exp(-iQ_1)$, $\exp(iQ_2)$, $\exp(-iQ_2)$. The trace of the product matrix is the sum of the eigenvalues, or $2\cos(Q_1)+2\cos(Q_2)$. The product of the two cosine terms can be found in a similar, but slightly more complicated way. In fact,

$$\cos(Q_1)+\cos(Q_2)=\tfrac{1}{2}(m_{11}+m_{22}+m_{33}+m_{44})\ , \quad (6a)$$

$$\begin{aligned}\cos(Q_1)\cos(Q_2)=\tfrac{1}{4}(&-2+m_{11}m_{22}+m_{11}m_{33}+m_{11}m_{44}\\ &+m_{22}m_{33}+m_{22}m_{44}+m_{33}m_{44}\\ &-m_{12}m_{21}-m_{13}m_{31}-m_{14}m_{41}\\ &-m_{23}m_{32}-m_{24}m_{42}-m_{34}m_{43})\ ,\end{aligned} \quad (6b)$$

where the m_{ij} refer to the elements of the product matrix. The solution of these two equations is made easier by the fact that the rhs of both equations are real. This is shown in the Appendix.

Once the two types of transfer matrices have been derived, the remaining calculations are limited to multiplication of four of these 4×4 matrices and finding the eigenvalues of the product, for every value of the energy. With the help of Eqs. (6) this is very easy and it comes essentially down to solving a second order polynominal. For this reason, the computational requirements are very modest.

III. APPLICATION TO Si-Ge_xSi_{1-x} SUPERLATTICES

In this section we will actually apply the method described in the previous section to Si-Ge_xSi_{1-x} superlattices. It has been shown, experimentally[27] and theoretically,[28] that for germanium concentrations $x \lesssim 0.2$ in the alloy, the conduction-band minimum is siliconlike, which means that it appears at Δ_1. Because we have disregarded the intrinsic curvature of the lowest band and were required to take the momentum matrix element T' equal in the two constituent materials, the data of Cardona and Pollak[20] cannot be used. The parameters we have used are given in Table I. The origin of energy is taken at the conduction-band minima. Note that as atomic units are used, the unit of energy is the Rydberg (13.6 eV), and the unit of length is the Bohr radius (0.0529 nm). Since we are primarily interested in the band structure around the conduction-band minimum, we have chosen our parameters with emphasis on the accuracy of the position of the

TABLE I. Parameters used for band structure of bulk materials. The origin of energy is taken at the valence-band minima.

Parameter	Si	Ge
$E(\Gamma_{15})$	0.2131	0.1931
$E(\Gamma_1^u)$	0.5386	0.5066
$E(\Gamma_1^l)$	−1.1314	−0.8595
T	1.382	1.382
T'	0.805	0.805

conduction-band minima and on the longitudinal effective mass.

For silicon we have used the well-known fact that the conduction-band minimum occurs at Δ_1 at about 85% of the edge of the Brillouin zone. For the longitudinal effective mass at the band minimum, we have used the results of Hensel *et al.*[29] For germanium the data is based on a local pseudopotential calculation using the form factors of Pandey and Phillips.[30] Table II gives the results. The band structure of silicon-germanium alloys has been obtained using the virtual-crystal approximation,[31] which means that the alloy band parameters are taken to be the weighted average of the parameters of the pure materials.

In Si-Ge_xSi_{1-x} SL's the situation is more complicated than in the bulk, as the lattice mismatch induced strain and the band offset have to be taken into account. The lattice constant of the SL is determined by the substrate or by a buffer layer on which the SL structure is grown. It can be different from the bulk lattice constants of either of the constituent materials, so that both materials can be under strain. The actual shape of the lowest conduction band does not change to first order in the strain, but rather it is shifted with respect to the other bands. The uniaxial component of the strain in the [100] direction causes the sixfold degenerate conduction-band minima to split into a doublet (the two minima in the direction of the strain) and a quartet (the four minima perpendicular to the strain). For negative uniaxial strain, the doublet is the lowest in energy. In this paper we neglect transverse effects and consequently do not take the quartet into account.

The band offset between the silicon and germanium valence bands have been determined recently by van de Walle and Martin.[32] Combining their results with phenomenological deformation potential theory, People and Bean[33,34] have obtained the band offsets of the conduction bands as well. The calculations by People and Bean indicate that depending on the choice of the parameters, the band alignment can be either straddled or staggered and the well for the electrons can be in either of the two materials. The splitting of the conduction band is described by the deformation potential Ξ_u, which has been measured by Balslev.[35] We have used his data valid at 80 K.

In giving examples of band structures, we have been led by Abstreiter *et al.*,[36] who have done extensive experiments with Si-$Ge_{0.5}Si_{0.5}$ SL's. The lattice constant of their samples is determined by a buffer layer with composition $Ge_{0.25}Si_{0.75}$. These authors propose a band line up in which the doublets in the silicon layers form the wells for the electrons. Based on the calculations by van de Walle and Martin,[32] People and Bean[34] come to the same conclusion and estimate the energy difference with the lowest alloy band, the quartets, to be 150 meV. Using Balslev's data[35] to obtain the quartet-doublet splitting, we finally obtain the band line up given in Fig. 2. It can be seen from this figure that doublets are 300 meV apart in energy and this is the band offset to be used for our SL band structure calculations. As the unit of length of the wells and barriers we have chosen the lattice constant in the SL direction. Notice that this quantity depends on the strain through Poisson's ratio, and will in general be different in the two materials.

TABLE II. Position of the conduction-band minimum and longitudinal effective mass as following from the parameters in Table I.

	Si	Ge
k_{min}	0.520	0.486
m_l	0.9163	0.908

Some results of band-structure calculations are given in Fig. 3. In this figure we have taken equal well and barrier sizes and we vary the total period of the system. It can be seen that the levels appear in pairs which seem to cross periodically. We have also done calculations based on Bastard's original work[13–15] for GaAs-based SL's in which we substituted the longitudinal effective masses of the constituent materials; in these calculations the indirect nature of the band gap of the bulk materials is neglected. It turns out that the results of these two calculations follow each other very closely. The difference is that applying the expression Bastard derives, one finds single energy levels, whereas in our calculations the levels appear in two closely spaced pairs as was mentioned above. In fact, the single energy levels as following from Bastard's work always lie in between the paired levels from our calculation, except in the immediate neighborhood of the crossover. This is a general feature that has been found to hold for all cases we have considered. For this reason we will not give any other examples in the present paper.

IV. DISCUSSION OF THE RESULTS

The splitting of the levels, as compared to those for SL's made of direct band gap materials is one of the most

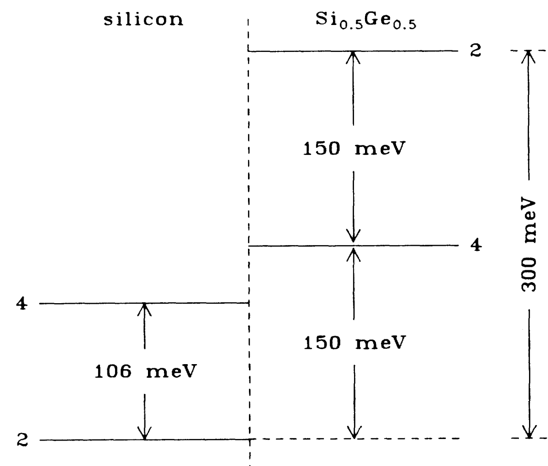

FIG. 2. Band lineup for Si-$Ge_{0.5}Si_{0.5}$ on a $Ge_{0.25}Si_{0.75}$ buffer layer. The "2" refers to the two degenerate conduction-band minima in the SL direction, and "4" refers to the four minima perpendicular to the SL direction.

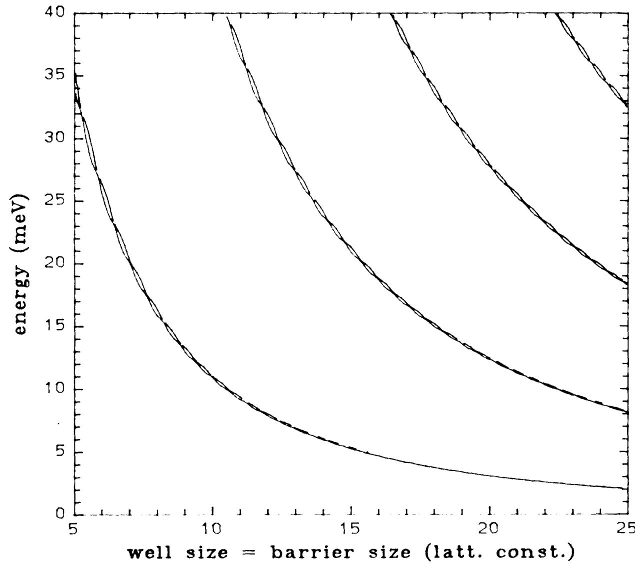

FIG. 3. Position of the energy levels for $Si-Ge_{0.5}Si_{0.5}$ SL on a $Ge_{0.25}Si_{0.75}$ buffer layer. The thicknesses of the wells and the barriers, measured in lattice constants, are taken equal. The origin of energy is the position of the conduction-band minima in the Si layers in the SL direction.

distinguishing features of our results. It can be understood in terms of a Fourier analysis of the system. If the energy is raised, starting at the minima of the conduction band in the bulk materials, four solutions for **k** will be found, two in each of the [100] minima. If a SL environment is now introduced, points that are exactly N (integer) SL reciprocal lattice vectors $(2\pi/d)$ away, will interact through the Nth Fourier component of the SL potential. Since the two minima are in so far apart in **k** space, the solutions in both of the minima will interact mutually through rather high Fourier components. The two solutions in each of the minima are much closer together and therefore interact through a low Fourier component. This last interaction is direct band-gap-like and is similar to what happens in GaAs-Al_xGa_{1-x}As SL's and hence gives a similar kind of band structure. It is the mutual interaction of the minima through the weaker high Fourier components that causes the levels in this band structure to split. This splitting is very similar to the valley-orbit splitting observed in shallow donor levels in silicon and germanium.[37]

It is quite revealing to consider the opposite situation, that of noninteracting barriers, as well. We will just take the simplest imaginable case: an infinite potential well for electrons in a siliconlike material. This problem can be solved very conveniently using the transfer matrix, derived in the Appendix. Since at both sides of the well the envelope functions must disappear, we take the first two elements of the vector **F**, Eq. (A5), to be zero, transfer over the width of the well, say w, and require that the vector thus obtained has the same property; this leads to the condition

$$\begin{bmatrix} 0 \\ 0 \\ F_1'(w) \\ F_2'(w) \end{bmatrix} = \underline{M}(w) \begin{bmatrix} 0 \\ 0 \\ F_1'(0) \\ F_2'(0) \end{bmatrix} . \tag{7}$$

This requirement can only be satisfied if the subdeterminant formed by the elements m_{13}, m_{14}, m_{23}, and m_{24} disappears. Substituting for the matrix $\underline{M}$ from Eq. (A6), we find after some algebraic manipulations, the following resonance condition for the energy E:

$$\cos[(k_1-k_2)w] - \tfrac{1}{2}\mu \sin(k_1 w)\sin(k_2 w) = 1 , \tag{8}$$

where

$$\mu = \frac{\varepsilon+k_2^2}{\varepsilon+k_1^2}\frac{k_1}{k_2} + \frac{\varepsilon+k_1^2}{\varepsilon+k_2^2}\frac{k_2}{k_1} - 2 , \tag{9}$$

and $\varepsilon = E(\Gamma_1^u)$ and $\pm k_1$ and $\pm k_2$ are the four solutions for **k** in the bulk material for the energy E. It is important for the forthcoming argument that since (in atomic units) $\varepsilon \approx 0.5$ and $k_1 \approx k_2 \approx 0.5$ (see Table II), $\mu \ll 1$. Equation (8) can be simplified if we assume that each of the minima has a parabolic shape. This is certainly a good approximation for the lower-lying energy levels. Then the average of k_1 and k_2 coincides with the minimum of the conduction band $k_{\min}$, independent of the energy. Writing Eq. (8) in terms of $k_{\min}$ and of $\Delta k = k_1 - k_2$, we obtain

$$\cos(\Delta k w) + \tfrac{1}{2}\mu \sin[(k_{\min}+\tfrac{1}{2}\Delta k)w]\sin[(k_{\min}-\tfrac{1}{2}\Delta k)w] = 1 . \tag{10}$$

For free electrons and for electrons in direct band-gap materials, the conventional case, $\mu=0$ and consequently $(\Delta k)w = 2\pi n$ (n integer; $n=0$ is not allowed). But even in our case, the second term forms only a small perturbation, since $\mu \ll 1$, and we therefore expand $(\Delta k)w$ around $2\pi n$. Retaining only the lowest terms in the expansion parameter and in μ, the following expression can be derived:

$$\Delta k = \frac{2\pi}{w}n \pm \frac{1}{w}\sqrt{\mu}\sin(k_{\min} w) . \tag{11}$$

So we see that, with respect to the conventional case, the number of solutions indeed has doubled. Using Eqs. (9) and (11), we can calculate the actual position of the energy levels. Again retaining only the lowest order terms we find

$$E = \frac{\pi^2 n^2}{m_l w^2}\left[1 \pm \zeta \frac{\sin(k_{\min} w)}{k_{\min} w}\right] . \tag{12}$$

where m_l is the (longitudinal) effective mass in the two minima ($m_l \approx 1$) and

$$\zeta = 2\left|\frac{\varepsilon - k_{\min}^2}{\varepsilon + k_{\min}^2}\right| . \tag{13}$$

The first term in Eq. (12) is the result for the conventional case; the second term represents the splitting of the levels. It is seen to be inversely proportional to the cube of the well width. For silicon, $k_{\min} \approx 0.5$ (see Table II), $\varepsilon \approx 0.5$,

and thus ζ is of the order of unity. Further, we set $w = aN$, where a is the lattice constant of the material ($a \approx 10$) and N is the width of the well in lattice constants. Unless N is very small therefore, $k_{\min} w \gg 1$ and consequently the second term in Eq. (12) is much smaller than unity and varies rapidly with the well width.

We have compared the predictions of Eqs. (12) and (13) with the calculated splittings for SL's, periodic structures with a finite barrier height. Figures 4 and 5 show magnified parts of the energy levels in Fig. 3. The vertical lines indicate the values of the well width for which $k_{\min} w = n\pi$ (n integer), so that the predicted splitting is zero. From Figs. 4 and 5 we can see that the vertical lines seem to be a bit off, but that their mutual distance is correct. This is a general feature and it has been confirmed for all cases we have investigated. The small displacement can be traced back to the application of the interface connection rules. If one assumes that the envelope functions and their derivatives are all continuous, so that one would use the unit matrix rather than the matrix in Eq. (4), the vertical lines coincide exactly with the positions of zero splitting. As to the amplitude of the splitting: for thick barrier layers the results of Eqs. (12) and (13) are essentially correct. For thin barriers, however, the predicted amplitude is too small compared to a full calculation. Clearly, tunneling, which is neglected in the calculation leading to Eqs. (12) and (13), plays a role for thin barrier layers.

The accuracy of our results is hard to estimate. The fact that our results and the results following from Bastard's work[13–15] are so similar is encouraging. Comparison with the tight-binding calculations of Krishnamurti and Moriarti[9–11] is impractical as their work does not predict the level splitting. These authors were primarily concerned with the enhancement of the electron mobility and consequently calculated only the position of the very lowest conduction bands.

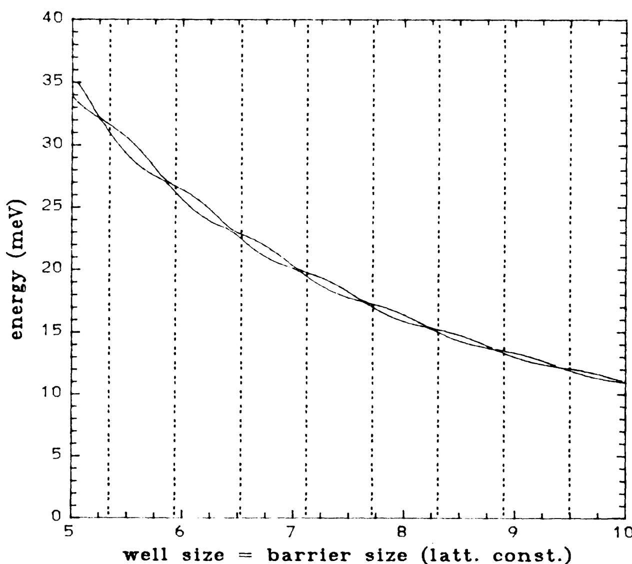

FIG. 4. Magnified part of Fig. 3. The dashed vertical lines indicate well widths for which Eq. (12) predicts zero splitting.

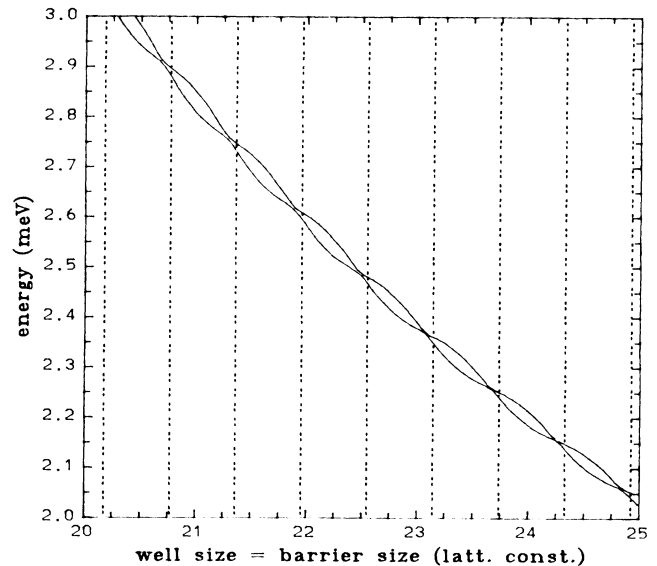

FIG. 5. Magnified part of Fig. 3. The dashed vertical lines indicate well widths for which Eq. (12) predicts zero splitting.

The experimental observation of the splitting will probably be difficult as it is fairly small and as it depends strongly on the well width. Thus interface imperfections and charge redistribution over the interfaces are likely to blur the splitting. Further, umklapp processes[37] are not taken into account in our calculations. In a SL, the perturbing potential is one dimensional so only valleys on the SL axis will contribute to these processes and not, as with donor impurities (which are intrinsically three dimensional), valleys in the fully three-dimensional reciprocal space. For this reason, we expect umklapp processes to be less prominent in a SL than in the donor impurity problem.

V. CONCLUSIONS

Our method shares the general advantages of the EFA over other methods for band-structure calculations for SL's in that it is simple and requires very modest calculations. This is especially true since we have been able to find analytic expressions for the transfer matrices. Moreover, the analytic expression for the materials transfer matrix has allowed us to obtain an expression for the energy levels in an infinite potential well made of an indirect band-gap material. This explained the variation of the level splitting we observed in the band structures.

We believe that this method can be extended to more general problems, for example for taking the transverse crystal momentum into account. As the complexity is increased, however, it will be more and more difficult to find analytic expressions for the material transfer matrices. This can be done numerically if necessary, but this would require extra computations, as this procedure has to be repeated for every value of the energy.

ACKNOWLEDGMENTS

The authors wish to thank S. Krishnamurti for sending them the results of the tight-binding calculations. One of

us (C.M.d.S.) is supported by the Corning Glassworks Foundation. This work is supported in part by the U.S. Joint Services Optics Program.

APPENDIX

In this appendix it will be shown how the transfer matrix for the materials can be found. For a certain energy, the solutions and first derivatives to Eq. (2) can be written as

$$\begin{aligned} F_1(x) &= -A\lambda_1 e^{ik_1x} + B\lambda_1 e^{-ik_1x} - C\lambda_2 e^{ik_2x} + D\lambda_2 e^{-ik_2x} , \\ F_2(x) &= +Ae^{ik_1x} + Be^{-ik_1x} + Ce^{ik_2x} + De^{-ik_2x} , \\ F_1'(x) &= -iA\lambda_1 k_1 e^{ik_1x} - iB\lambda_1 k_1 e^{-ik_1x} \\ &\quad - iC\lambda_2 k_2 e^{ik_2x} - iD\lambda_2 k_2 e^{-ik_2x} , \\ F_2'(x) &= +iAk_1 e^{ik_1x} - iBk_1 e^{-ik_1x} \\ &\quad + iCk_2 e^{ik_2x} - iDk_2 e^{-ik_2x} , \end{aligned} \tag{A1}$$

where

$$\lambda_i = \frac{k_i^2 + [E(\Gamma_1^u) - E]}{Tk_i} , \tag{A2}$$

and k_1 and k_2 are found by solving the associated characteristic equation. It follows directly from Eqs. (A1) that

$$\begin{aligned} F_1(0) &= -\lambda_1 A + B\lambda_1 - C\lambda_2 + D\lambda_2 , \\ F_2(0) &= +A + B + C + D , \\ F_1'(0) &= -i\lambda_1 k_1 A - i\lambda_1 k_1 B - i\lambda_2 k_2 C - i\lambda_2 k_2 D , \\ F_2'(0) &= ik_1 A - ik_1 B + ik_2 C - ik_2 D . \end{aligned} \tag{A3}$$

The next step is to substitute $F_1(0)$, $F_1'(0)$, $F_2(0)$, $F_2'(0)$ for A, B, C, D in Eq. (A1) using Eq. (A3). For this particular problem, we have been able to do this analytically. The result can be written as

$$\mathbf{F}(x) = \underline{M}(x)\mathbf{F}(0) , \tag{A4}$$

where $\mathbf{F}$ is the column matrix with elements

$$(F_1(x), F_2(x), F_1'(x), F_2'(x))^T . \tag{A5}$$

The elements of the matrix $M(x)$ are

$$\begin{aligned} m_{11} &= [-k_2^2(\varepsilon+k_1^2)C_1 + k_1^2(\varepsilon+k_2^2)C_2]/[\varepsilon(k_1^2-k_2^2)] , \\ m_{12} &= i(\varepsilon+k_1^2)(\varepsilon+k_2^2)(k_2 s_1 - k_1 S_2)/[k_1 k_2 T(k_1^2-k_2^2)] , \\ m_{13} &= [k_2(\varepsilon+k_1^2)S_1 - k_1(\varepsilon+k_2^2)S_2]/[k_1 k_2(k_1^2-k_2^2)] , \\ m_{14} &= i(\varepsilon+k_1^2)(\varepsilon+k_2^2)(C_1-C_2)/[T\varepsilon(k_1^2-k_2^2)] , \\ \\ m_{21} &= iTk_1k_2(k_2S_1-k_1S_2)/[\varepsilon(k_1^2-k_2^2)] , \\ m_{22} &= [-(\varepsilon+k_2^2)C_1 + (\varepsilon+k_1^2)C_2]/(k_1^2-k_2^2) , \\ m_{23} &= iT(C_1-C_2)/(k_1^2-k_2^2) , \\ m_{24} &= [k_1(\varepsilon+k_2^2)S_1 - k_2(\varepsilon+k_1^2)S_2]/[\varepsilon(k_1^2-k_2^2)] , \\ \\ m_{31} &= k_1k_2[k_2(\varepsilon+k_1^2)S_1 - k_1(\varepsilon+k_2^2)S_2]/[\varepsilon(k_1^2-k_2^2)] , \\ m_{32} &= i(\varepsilon+k_1^2)(\varepsilon+k_2^2)(C_1-C_2)/[T(k_1^2-k_2^2)] , \\ m_{33} &= [(\varepsilon+k_1^2)C_1 - (\varepsilon+k_2^2)C_2]/(k_1^2-k_2^2) , \\ m_{34} &= -i(\varepsilon+k_1^2)(\varepsilon+k_2^2)(k_1S_1-k_2S_2)/[T\varepsilon(k_1^2-k_2^2)] , \\ \\ m_{41} &= ik_1^2k_2^2T(C_1-C_2)/[\varepsilon(k_1^2-k_2^2)] , \\ m_{42} &= [k_1(\varepsilon+k_2^2)S_1 - k_2(\varepsilon+k_1^2)S_2]/(k_1^2-k_2^2) , \\ m_{43} &= -iT(k_1S_1-k_2S_2)/(k_1^2-k_2^2) , \\ m_{44} &= [k_1^2(\varepsilon+k_2^2)C_1 - k_2^2(\varepsilon+k_1^2)C_2]/[\varepsilon(k_1^2-k_2^2)] , \end{aligned} \tag{A6}$$

where $S_i = \sin(k_i x)$ and $C_i = \cos(k_i x)$ and $\varepsilon = [E(\Gamma_1^u) - E]$.

Note that the matrix elements with two even and the elements with two odd indices are real, whereas the remaining elements are purely imaginary (this is also true if k_i is complex). It can be seen from Eq. (4) that the interface transfer matrix has the same property, and therefore also any product of these matrices. For this reason, the rhs of Eq. (6) are real, and hence also the sum and the product of the two cosine terms [Eq. (6)], as was claimed in Sec. II.

[1] L. Esaki and R. Tsu, IBM J. Res. Develop. **40**, 61 (1970).
[2] *Synthetic Modulated Structures*, edited by L. L. Chang and B. C. Giessen (Academic, Orlando, 1985).
[3] *Molecular Beam Epitaxy and Heterostructures*, edited by L. L. Chang and K. Ploog (Martinus Nijhoff, Dordrecth, 1985).
[4] H. M. Manasevit, I. S. Gergis, and A. B. Jones, Appl. Phys. Lett. **41**, 464 (1982).
[5] J. C. Beam, L. C. Feldman, A. T. Fiory, S. Nakahara, and I. K. Robinson, J. Vac. Sci. Technol. A **2**, 436 (1984).
[6] R. People, J. C. Bean, D. V. Lang, A. M. Sergent, H. L. Störmer, K. W. Wecht, R. T. Lynch, and K. Baldwin, Appl. Phys. Lett. **45**, 1231 (1984).
[7] R. Hull, J. M. Gibson, and J. C. Bean, Appl. Phys. Lett. **46**, 179 (1985).
[8] D. Mukherji and B. R. Nag, Phys. Rev. B **12**, 4338 (1975).
[9] J. A. Moriarti and S. Krishnamurti, J. Appl. Phys. **54**, 1892 (1983).
[10] S. Krishnamurti and J. A. Moriarti, Superlatt. Microstruct. **1**, 209 (1985).
[11] S. Krishnamurti and J. A. Moriarti, Phys. Rev. B **32**, 1027 (1985).
[12] J. N. Schulman and Y. C. Chang, Phys. Rev. B **24**, 4445 (1981).
[13] G. Bastard, in *Molecular Beam Epitaxy and Heterostructures*, Ref. 3, Chap. 11.
[14] G. Bastard, Phys. Rev. B **24**, 5693 (1981).
[15] G. Bastard, Phys. Rev. B **25**, 7584 (1982).
[16] M. F. H. Schuurmans and G. W. 't Hooft, Phys. Rev. B **31**,

8041 (1985).
[17]J. Callaway, *Quantum Theory of the Solid State* (Academic, New York, 1974), Part A, p. 246.
[18]J. M. Luttinger and W. Kohn, Phys. Rev. **97**, 869 (1955).
[19]E. O. Kane, in *Handbook on Semiconductors* (North-Holland, New York, 1982), Vol. 1, p. 193.
[20]M. Cardona and F. H. Pollak, Phys. Rev. **142**, 530 (1966).
[21]V. Heine, Proc. Phys. Soc. London **81**, 300 (1963).
[22]Y. C. Chang, Phys. Rev. B **25**, 605 (1982).
[23]Y. C. Chang and J. N. Schulman, Phys. Rev. B **25**, 3975 (1982).
[24]R. A. Smith, *Wave Mechanics of Crystalline Solids* (Chapman & Hall, London, 1969), Chap. 4.
[25]H. M. James and A. S. Ginzbarg, J. Phys. Chem. **37**, 840 (1953).
[26]L. J. Sham and M. Nakayama, Phys. Rev. B **20**, 734 (1979).
[27]R. Braunstein, A. R. Moore, and F. Herman, Phys. Rev. **109**, 695 (1958).
[28]K. E. Newman and J. D. Dow, Phys. Rev. B **30**, 1929 (1984).
[29]J. C. Hensel, H. Hasegawa, and M. Nakayama, Phys. Rev. **138**, A225 (1965).
[30]K. C. Pandy and J. C. Phillips, Phys. Rev. B **9**, 1552 (1974).
[31]R. H. Parmenter, Phys. Rev. **97**, 587 (1955).
[32]C. G. van de Walle and R. M. Martin, J. Vac. Sci. Technol. B **3**, 1256 (1985).
[33]R. People, Phys. Rev. B **32**, 1405 (1985).
[34]R. People and J. C. Bean, Appl. Phys. Lett. **48**, 538 (1986).
[35]I. Balslev, Phys. Rev. **143**, 636 (1966).
[36]G. Abstreiter, H. Brugger, T. Wolf, H. Jorke, and H. J. Herzog, Phys. Rev. Lett. **54**, 2441 (1985).
[37]M. Altarelli and F. Bassani, in *Handbook on Semiconductors*, edited by T. S. Moss (North-Holland, New York, 1982), Vol. 1, p. 269.